Charge density waves in kagome-lattice extended Hubbard models at the van Hove filling

Francesco Ferrari,[1] Federico Becca,[2] and Roser Valentí[1]
[1]*Institute for Theoretical Physics, Goethe University Frankfurt, Max-von-Laue-Straße 1, D-60438 Frankfurt am Main, Germany*
[2]*Dipartimento di Fisica, Università di Trieste, Strada Costiera 11, I-34151 Trieste, Italy*

The Hubbard model on the kagome lattice is presently often considered as a minimal model to describe the rich low-temperature behavior of AV_3Sb_5 compounds (with $A = \mathrm{K}, \mathrm{Rb}, \mathrm{Cs}$), including charge density waves (CDWs), superconductivity, and possibly broken time-reversal symmetry. Here, we investigate, via variational Jastrow-Slater wave functions, the properties of its ground state when both on-site U and nearest-neighbor V Coulomb repulsions are considered at the van Hove filling. Our calculations reveal the presence of different interaction-driven CDWs and, contrary to previous renormalization-group studies, the absence of ferromagnetism and charge- or spin-bond order. No signatures of chiral phases are detected. Remarkably, the CDWs triggered by the nearest-neighbor repulsion possess charge disproportionations that are not compatible with the ones observed in AV_3Sb_5. As an alternative mechanism to stabilize charge-bond order, we consider the electron-phonon interaction, modeled by coupling the hopping amplitudes to quantum phonons, as in the Su-Schrieffer-Heeger model. Our results show the instability towards a trihexagonal distortion with 2×2 periodicity, in closer agreement with experimental findings.

Introduction. The interplay between electronic correlation and lattice geometry is the source of several fundamental phenomena in condensed-matter systems. The Hubbard model, with nearest-neighbor hopping amplitude t and on-site repulsion U [1], represents the simplest way to describe interacting electrons in a crystal. The competition between the kinetic processes and the Coulomb interaction is enhanced on frustrated lattices, giving rise to a rich physical behavior. In two dimensions, a particularly interesting case is represented by the kagome lattice, for which a few studies have focused on the Mott transition at half filling [2–7]. Extended Hubbard models on the kagome lattice involving the nearest-neighbor interactions V have been explored as well, such as the case of spinless fermions at $1/3$ filling, where the Fermi energy lies at the Dirac points of the noninteracting band structure [8–12]. Within the spinful case, some attention has been given to the model at $5/6$ filling, where the Fermi energy intersects a van Hove singularity [13–16]. This scenario is particularly interesting because the Bloch states connected by the nesting vectors display different sublattice characters, thus obstructing the onset of electronic instabilities generated by the Hubbard-U interaction, which acts on the same sublattice [14]. Therefore the nearest-neighbor V term can play an important role. Indeed, renormalization-group analyses have shown the appearance of several unconventional electronic phases, including ferromagnetism and charge- or spin-bond orders, although considerably different phase diagrams have been obtained by two independent calculations [15,16].

A renovated interest in the properties of the kagome-lattice system at the van Hove filling has been sparked by the recent discovery of the family of AV_3Sb_5 metals (with $A = \mathrm{K}, \mathrm{Rb}, \mathrm{Cs}$) [17]. Their *ab initio* electronic band structure displays different van Hove singularities in the proximity of the Fermi energy, originating from the d orbitals of vanadium atoms, which form almost perfect two-dimensional kagome layers. Upon lowering the temperature, AV_3Sb_5 materials undergo two subsequent transitions [18], first developing charge density wave (CDW) order in an intermediate regime [19–25] and then exhibiting superconductivity at lower temperatures [26–29]. The CDW phase requires a 2×2 supercell within the vanadium layers [19,20], with star-of-David and/or trihexagonal patterns [30,31]. Interestingly, different experimental probes have detected signatures of time-reversal symmetry breaking in the CDW phase, stimulating the understanding of its origin [19,24,32–36].

The starting point of most theoretical studies is the Hubbard model on the kagome lattice with a single orbital per site, originating from the d_{xy} orbitals of the vanadium atoms [19,37,38]. Within this minimal formulation, different CDW phases have been proposed to arise as potential instabilities of the electronic band structure at the van Hove filling, some of them featuring nontrivial orbital currents [39–44]. The microscopic physical mechanism triggering the CDW instability is still under debate. While an early mean-field analysis has indicated the nearest-neighbor electronic repulsion as the possible origin of the chiral CDW observed in AV_3Sb_5 [37], several works suggest that lattice deformations and electron-phonon coupling may play an important role [45–52].

Motivated by these studies, we revisit the problem of the extended Hubbard model on the kagome lattice at the van Hove filling, with U and V terms. We employ a variational Monte Carlo approach based on Jastrow-Slater wave functions to map out the phase diagram of the model and analyze the CDW instabilities induced by the electronic repulsion.

Our results show that different CDWs can be stabilized in the phase diagram, but no ferromagnetism is present. In addition, charge- or spin-bond order is detected only within uncorrelated states (i.e., without the Jastrow factor), while the correlated Jastrow-Slater wave functions do not show any evidence for this kind of instabilities. Our outcomes are in striking contrast to previous calculations based on functional renormalization group approaches [15,16]. Most importantly, charge modulations generated by the Coulomb repulsion V display a substantial disproportionation on neighboring sites, which is not compatible with the 2×2 CDW observed experimentally [19–23,25], where the electron density retains an almost perfect C_6 rotational symmetry around the center of hexagons (forming star-of-David or trihexagonal patterns). For this reason, we also analyze the effect of the electron-phonon coupling on the Hubbard model (without V), where phonons affect hopping amplitudes, as in the Su-Schrieffer-Heeger model [53]. In this case, lattice distortions appear, with short bonds along disconnected hexagons, favoring a charge reorganization that is similar to the one observed in AV_3Sb_5 [30,31].

The purely electronic model. We consider the (extended) Hubbard model for spinful electrons on the kagome lattice

$$\mathcal{H} = -t \sum_{\langle i,j\rangle,\sigma} (c^{\dagger}_{i,\sigma} c_{j,\sigma} + \text{H.c.}) + U \sum_{i} n_{i,\uparrow} n_{i,\downarrow} + V \sum_{\langle i,j\rangle} n_i n_j, \qquad (1)$$

where $t > 0$ is the nearest-neighbor hopping term and $U \geqslant 0$ and $V \geqslant 0$ denote the strength of the on-site and nearest-neighbor repulsive interactions, respectively. The fermionic operator $c_{i,\sigma}$ ($c^{\dagger}_{i,\sigma}$) annihilates (creates) an electron with spin σ on site i. The Coulomb interactions are expressed in terms of the number operators $n_{i,\sigma} = c^{\dagger}_{i,\sigma} c_{i,\sigma}$ and $n_i = n_{i,\uparrow} + n_{i,\downarrow}$. The total number of sites in the system is denoted by N, while the total number of electrons is $N_e = N_\uparrow + N_\downarrow$, with $N_\sigma = \sum_i n_{i,\sigma}$. In the following, we focus on the filling $n_F = N_e/N = 5/6$, for which the noninteracting Fermi energy intersects the upper van Hove singularity [54].

We investigate the Hamiltonian of Eq. (1) by a variational approach, which relies on the use of Jastrow-Slater wave functions to approximate the ground state of the Hubbard model, and Monte Carlo sampling to stochastically compute observables. Our variational *Ansätze* take the general form $|\Psi_e\rangle = \mathcal{J}|\Phi_0\rangle$, in which a long-range density-density Jastrow factor

$$\mathcal{J} = \exp\left(\sum_{i,j} v_{i,j} n_i n_j\right) \qquad (2)$$

is applied on top of an uncorrelated fermionic state, $|\Phi_0\rangle$, to introduce nontrivial correlations between electrons. The resulting wave function goes beyond standard mean-field approaches based on uncorrelated states and can potentially describe different phases of Hubbard-like models [55–60], e.g., metallic and (Mott or band) insulating phases. We take the uncorrelated part of the variational state, $|\Phi_0\rangle$, to be the ground state of an auxiliary tight-binding Hamiltonian

$$\mathcal{H}_0 = -\sum_{\langle i,j\rangle,\sigma} T^{\sigma}_{i,j} (c^{\dagger}_{i,\sigma} c_{j,\sigma} + \text{H.c.}) - \sum_i \mu_i c^{\dagger}_{i,\sigma} c_{i,\sigma}, \qquad (3)$$

featuring nearest-neighbor hopping terms ($T^{\sigma}_{i,j}$) and on-site potentials (μ_i). The parameters of $\mathcal{H}_0$ are optimized together with the (translationally invariant) $v_{i,j}$ parameters defining the Jastrow factor, to minimize the variational energy of $|\Psi_e\rangle$. The optimization is performed numerically by means of the stochastic reconfiguration technique [61]. Further details on the variational calculations are reported in the Supplemental Material [54].

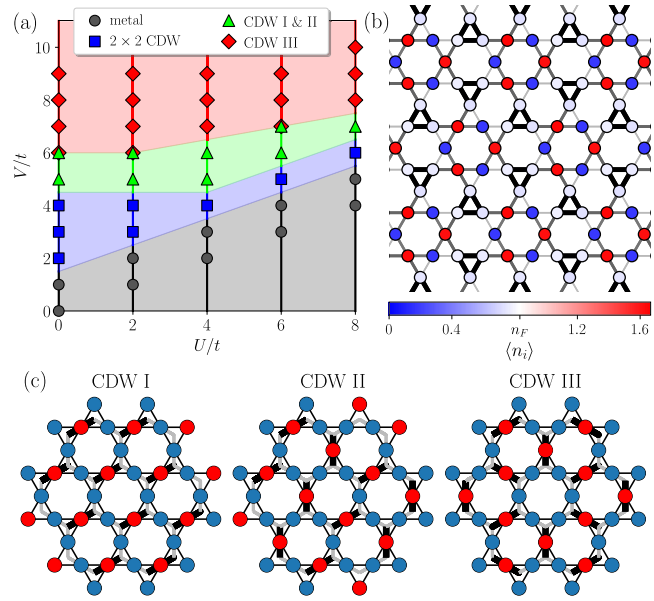

FIG. 1. (a) Phase diagram of the Hubbard model of Eq. (1) at the van Hove filling $n_F = 5/6$. The symbols indicate the values of U/t and V/t for which the calculations have been performed (on finite-sized lattices with $L_1 = 12$ and $L_2 = 10$ and 18 [54]). Overlapping symbols are used when the variational energies of two phases are equivalent within error bars. (b) Charge pattern in the 2×2 CDW phase. The color of each site i indicates the average number of electrons $\langle n_i \rangle$, while the width and the darkness of the lines connecting nearest neighbors (i, j) are proportional to the modulus of the expectation value of the hopping operator along the bond, namely, $|\langle c^{\dagger}_{i,\uparrow} c_{j,\uparrow} + c^{\dagger}_{i,\downarrow} c_{j,\downarrow} \rangle|$. Results for $U/t = 0$ and $V/t = 3$ are shown. (c) Sketch of the electronic charge patterns of the CDW I, II, and III phases, fulfilling the *triangle rule*. Blue (red) circles denote depletion (accumulation) of electrons. Following Ref. [9], for each CDW we show the dimer configuration on the honeycomb lattice formed by connecting the centers of the corner-sharing triangles.

Results. The phase diagram of the model, as obtained by our variational approach, is shown in Fig. 1(a), featuring a metallic phase for (relatively) small values of V/t and different CDW phases, illustrated in Figs. 1(b) and 1(c), which are stabilized by the presence of a sizable nearest-neighbor interaction.

The variational *Ansatz* for the metallic phase is obtained by applying the Jastrow factor $\mathcal{J}$ (2) on top of the uncorrelated ground state of the uniform auxiliary Hamiltonian of Eq. (3) with $T^{\sigma}_{i,j} = 1$ at nearest neighbors and $\mu_i = 0$ for all sites. The

resulting wave function, which reduces to the exact ground state of the model in the noninteracting limit ($U = V = 0$), turns out to provide the optimal variational energy in the whole metallic phase [gray region in Fig. 1(a)]. No sign of ferromagnetism is observed in the metallic region, in contrast to previous renormalization-group results [15,16]. Indeed, by performing the variational calculations for different values of the magnetization $m = (N_\uparrow - N_\downarrow)/N$, the minimal energy is always found to be at $m = 0$ (while the uncorrelated wave function, with no Jastrow factor, gives a finite magnetization in a portion of the phase diagram [54]).

The inclusion of a sizable nearest-neighbor Hubbard interaction V induces the onset of charge order. Within our variational approach, we can define CDW phases and charge-bond ordered (CBO) phases by suitable choices for the auxiliary Hamiltonian $\mathcal{H}_0$. For CDW states, $\mathcal{H}_0$ contains a uniform nearest-neighbor hopping ($T^\sigma_{i,j} = 1$) and nonzero on-site potentials μ_i. Instead, CBO states are obtained when the hoppings $T^\sigma_{i,j}$ of $\mathcal{H}_0$ take different values on different bonds, breaking the symmetries of the kagome lattice. In contrast to renormalization-group results [15,16], our variational phase diagram contains only CDW phases driven by the on-site accumulation or depletion of electronic charge. No CBO phases are observed. In order to determine the optimal CDW states, we performed several numerical calculations in which the on-site potentials μ_i have been taken to be periodic over different supercells.

The first CDW phase induced by the nearest-neighbor repulsion requires a 2×2 supercell (containing 12 sites), which breaks the translational symmetry of the kagome lattice [blue region in Fig. 1(a)]. The charge pattern of this CDW, depicted in Fig. 1(b), is characterized by hexagons whose vertices show an alternating excess ($\langle n_i \rangle > n_F$) and deficiency ($\langle n_i \rangle < n_F$) of the local electron density, surrounded by triangles with a tiny electronic depletion. Thus the 2×2 CDW state breaks the D_6 point group symmetry of the kagome lattice down to D_3. This CDW phase is insulating, as testified by the presence of a finite gap in the energy spectrum of the auxiliary Hamiltonian $\mathcal{H}_0$. A further confirmation comes from the calculation of the small-q behavior of the density-density structure factor $N(\vec{q}\,)$ [54–56].

When the nearest-neighbor interaction is further increased, we detect the transition towards a set of different CDWs, which are characterized by a common feature, namely, they satisfy a *triangle rule* [9]: Each unit cell of the kagome lattice contains one site where $\langle n_i \rangle > n_F$ (electron accumulation) and two sites where $\langle n_i \rangle < n_F$ (electron depletion). Furthermore, the repulsive interaction V selects the extended charge patterns in which electron-rich sites are surrounded only by electron-poor sites at nearest neighbors. Analogous patterns have been observed in the phase diagram of the interacting spinless fermions at 1/3 filling [10]. Here, the CDW states satisfying the *triangle rule* can be visualized as hard-core dimer configurations on the honeycomb lattice, which is formed by the centers of corner-sharing triangular plaquettes [9]. Three relevant charge patterns of this kind, dubbed CDW I, II, and III, are shown in Fig. 1(c). For large values of V, the CDW III order with a $\sqrt{3} \times \sqrt{3}$ supercell turns out to be the ground state of the system [red region in Fig. 1(a)]. For intermediate values of V/t, sandwiched between the 2×2 CDW and the CDW III phases, we find a region in the phase diagram where the lowest variational energy is given by the CDW I and II orders [green region in Fig. 1(a)]. Actually, within this phase, not only do these two CDWs yield the same variational energy, but also they turn out to be degenerate with other possible patterns in which CDW I and II orders coexist in different portions of the lattice. We remark that all the CDWs satisfying the *triangle rule* are gapless, as inferred from the energy spectrum of the auxiliary Hamiltonian and the behavior of the structure factor $N(\vec{q}\,)$ [54].

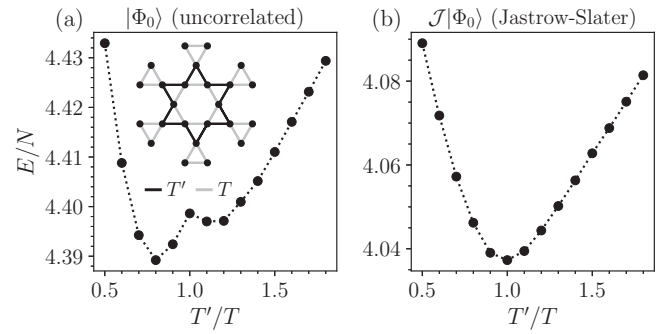

FIG. 2. Variational energy landscape of a wave function reproducing the 2×2 CBO of Ref. [15], for $U/t = 8$ and $V/t = 4$. The energy is plotted as a function of the ratio between the hopping parameters of $\mathcal{H}_0$ for the nearest-neighbor bonds inside (T') and outside (T) the star of David (shown in the inset). Results for the uncorrelated state $|\Phi_0\rangle$ (a) and the correlated one $\mathcal{J}|\Phi_0\rangle$ (b) are shown. The error bars are smaller than the size of the symbols. The calculations have been performed on a finite lattice with $L_1 = 12$ and $L_2 = 10$ [54].

As previously mentioned, while renormalization-group calculations detect the presence of CBO and spin-bond order (SBO) in the phase diagram, our variational results show that only CDW phases are stabilized by the presence of the nearest-neighbor interaction. To further investigate the possibility of bond order, we consider two variational *Ansätze* that can reproduce the CBO and SBO phases of Ref. [15]. These are characterized by a 2×2 supercell and a star-of-David pattern for the bond correlations. For the CBO state, we take two distinct (spin-isotropic) hopping parameters within $\mathcal{H}_0$, $T' > 0$ and $T > 0$, for the nearest-neighbor bonds inside and outside the star of David sketched in Fig. 2(a). Interestingly, CBO order is present when the uncorrelated wave function is employed, with the energy landscape having a minimum for $T' \neq T$ [Fig. 2(a)]. However, when the Jastrow factor is included to insert electron correlation, the minimum shifts to $T' = T$, indicating that there is no CBO [see Fig. 2(b)]. A similar analysis can be done to study the possible insurgence of SBO, imposing spin-dependent hoppings and taking $T_\uparrow \leqslant T_\downarrow$ ($T_\uparrow \geqslant T_\downarrow$) inside (outside) the star of David. Also in this case, a finite order is present only in the uncorrelated state, while, in the presence of the Jastrow factor, no order is present [54].

Finally, we emphasize that we did not detect the presence of chiral charge order in the phase diagram of the model. To describe nontrivial orbital currents and chiral order, we considered variational *Ansätze* in which the auxiliary Hamiltonian $\mathcal{H}_0$ includes complex hopping terms, following the patterns discussed in previous works [37,39,41,43]. Within the range

of couplings considered in this Research Letter, we find that the complex hopping parameters do not provide any improvement of the variational energy, thus implying the absence of interaction-driven chiral charge order in the ground state of the model [54].

Electron-phonon coupling. The 2×2 CDW that has been obtained within the extended Hubbard model [see Fig. 1(b)] can hardly be reconciled with the one observed in AV_3Sb_5, where the charge shows star-of-David and/or trihexagonal patterns. This outcome suggests that the origin of the charge disproportionation in these materials may not be purely electronic and phonons could play an important role. To elucidate this aspect, we consider a Su-Schrieffer-Heeger model in which hoppings between electrons are linearly coupled to lattice distortions. The lattice degrees of freedom are described by a set of uncoupled harmonic oscillators centered on the lattice sites (Einstein phonons). In addition, the Hubbard U is considered, leading to

$$\mathcal{H}_{\rm ep} = \sum_{\langle i,j\rangle,\sigma} \left[-t + \alpha \frac{\vec{r}_{i,j}}{||\vec{r}_{i,j}||} \cdot (\vec{u}_i - \vec{u}_j) \right] c^\dagger_{i,\sigma} c_{j,\sigma} + \text{H.c.} + \sum_i \left(\frac{1}{2m} \vec{p}_i^{\,2} + \frac{1}{2} m\omega^2 \vec{u}_i^{\,2} \right) + U \sum_i n_{i,\uparrow} n_{i,\downarrow}. \quad (4)$$

Here, $\vec{u}_i = (x_i, y_i)$ and $\vec{p}_i = (p_i^x, p_i^y)$ are the displacement and momentum operators of the Einstein phonons. The vectors $\vec{r}_{i,j} = (\vec{r}_i - \vec{r}_j)$ measure the difference in sites' positions in the undistorted kagome lattice. The phonon frequency and the mass of the ions are denoted by ω and m, respectively, and the strength of the electron-phonon coupling is controlled by the parameter $\alpha > 0$ or, equivalently, by the dimensionless parameter $\lambda = \alpha^2/(m\omega^2 t)$ [62].

We employ a variational wave function that includes both electronic and phononic degrees of freedom [63,64]

$$|\Psi_{\rm ep}\rangle = \mathcal{J}_{\rm ep} |\Psi_{\rm e}\rangle \otimes |\Psi_{\rm p}\rangle, \quad (5)$$

where $|\Psi_{\rm e}\rangle$ is the Jastrow-Slater wave function for the electrons, $|\Psi_p\rangle$ is a phonon coherent state, and $\mathcal{J}_{\rm ep}$ is an additional Jastrow factor that couples electron and phonon degrees of freedom. For the electron wave function, we fully optimize the hoppings of the auxiliary Hamiltonian $\mathcal{H}_0$ within a 2×2 supercell. The phonon wave function $|\Psi_p\rangle$ is a product of Gaussians in the basis of displacements $\vec{u}_i$

$$\langle \{\vec{u}_i\} | \Psi_p \rangle = \prod_i \exp\left\{ -\frac{m\omega}{2\hbar} [(x_i - X_i)^2 + (y_i - Y_i)^2] \right\}, \quad (6)$$

where X_i and Y_i are variational parameters that control the presence of finite distortions. The electron-phonon Jastrow factor reads

$$\mathcal{J}_{\rm ep} = \exp\left\{ \sum_{i,j} n_i n_j \left[w^x_{i,j} (x_i - x_j) + w^y_{i,j} (y_i - y_j) \right] \right\}. \quad (7)$$

The variational parameters $w^x_{i,j}$ and $w^y_{i,j}$ depend only on the distance between lattice sites, $||\vec{r}_{i,j}||$, and are odd under the exchange $i \leftrightarrow j$. To compute observables, we use a Monte Carlo approach to sample the infinite Hilbert space of the system in the basis of electron occupancies and site displacements, i.e., $\{|n_i\rangle \otimes |\vec{u}_i\rangle\}$.

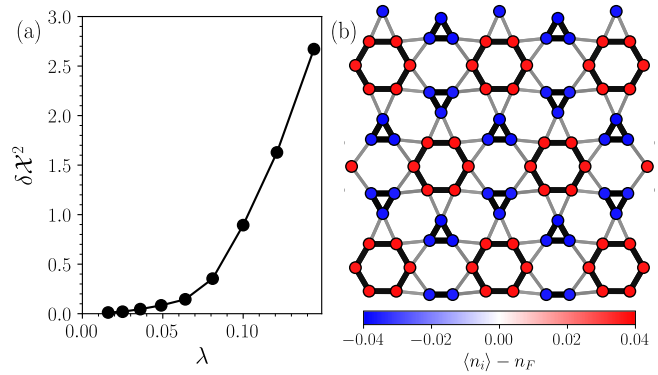

FIG. 3. (a) Mean-square displacement $\delta\mathcal{X}^2$ as a function of the electron-phonon coupling λ in the trihexagonal distorted phase of $\mathcal{H}_{\rm ep}$. (b) Lattice distortion induced by the electron-phonon coupling at $\lambda \approx 0.14$. The color of the sites represents the difference of the local electron density with respect to the filling, $\langle n_i \rangle - n_F$. The width and the darkness of (i, j) bonds are proportional to $|\langle c^\dagger_{i,\uparrow} c_{j,\uparrow} + c^\dagger_{i,\downarrow} c_{j,\downarrow} \rangle|$. The calculations have been performed on a finite lattice with $L_1 = 8$ and $L_2 = 6$ [54].

The results for $\hbar\omega/t = 0.05$ and $U/t = 4$, by varying the electron-phonon coupling λ, are shown in Fig. 3. We report a measure of the mean-square displacement, $\delta\mathcal{X}^2 = 1/N \sum_i \langle \Psi_{\rm ep} | \tilde{u}_i^2 | \Psi_{\rm ep} \rangle$ (where $\tilde{u}_i^2 = 2m\omega \vec{u}_i^{\,2}/\hbar$), and the local electron density. For large enough λ, the system develops a trihexagonal lattice distortion with CBO (also referred to as *inverse star of David* [48]), characterized by shrunk hexagons with accumulation of electrons, surrounded by shrunk triangles with electron depletion (see Fig. 3). The resulting CDW state is insulating. Still, the charge modulation of the distorted phase is in closer agreement with reported scanning tunneling microscopy measurements for AV_3Sb_5 [19,20], supporting the fact that an electron-phonon mechanism, rather than longer-range electronic repulsions, may be at the origin of the the 2×2 charge order observed in these materials.

Conclusions. We have analyzed the extended Hubbard model on the kagome lattice, with a single orbital on each site, including either the nearest-neighbor interaction V or the electron-phonon coupling λ, which can be taken as the simplest possible approximation to capture some aspects of AV_3Sb_5 compounds. Both V and λ may stabilize CDW with a 2×2 supercell; however, the charge pattern obtained from V is characterized by a sizable C_6 to C_3 rotational breaking of hexagons, which can hardly be reconciled with experiments on AV_3Sb_5. A more realistic charge reorganization is found by invoking a phonon mechanism. The present results indicate that CDW formation can be described within a minimal model where the multiorbital character can be neglected. Still, the resulting CDW is insulating, and no sign of either interaction-driven or phonon-driven time-reversal breaking is observed. These facts strongly suggest that the metallic and chiral properties have a different origin, which should be ascribed to other degrees of freedom (e.g., antimony atoms or additional vanadium orbitals) and physical mechanisms (e.g., spin-orbit coupling).

Acknowledgments. We are grateful to S. Backes, S. Bhattacharyya, K. Riedl, P. Wunderlich, and R. Thomale for insightful discussions. F.F. acknowledges support from the Alexander von Humboldt Foundation through a postdoctoral Humboldt fellowship. F.F. and R.V. acknowledge support by the Deutsche Forschungsgemeinschaft (DFG, German Research Foundation) for funding through TRR 288 – 422213477 (project A05).

[1] J. Hubbard, Proc. R. Soc. London, Ser. A **276**, 238 (1963).
[2] N. Bulut, W. Koshibae, and S. Maekawa, Phys. Rev. Lett. **95**, 037001 (2005).
[3] T. Ohashi, N. Kawakami, and H. Tsunetsugu, Phys. Rev. Lett. **97**, 066401 (2006).
[4] S. Kuratani, A. Koga, and N. Kawakami, J. Phys.: Condens. Matter **19**, 145252 (2007).
[5] S. Guertler, Phys. Rev. B **90**, 081105(R) (2014).
[6] R.-Y. Sun and Z. Zhu, Phys. Rev. B **104**, L121118 (2021).
[7] J. Kaufmann, K. Steiner, R. T. Scalettar, K. Held, and O. Janson, Phys. Rev. B **104**, 165127 (2021).
[8] S. Nishimoto, M. Nakamura, A. O'Brien, and P. Fulde, Phys. Rev. Lett. **104**, 196401 (2010).
[9] A. O'Brien, F. Pollmann, and P. Fulde, Phys. Rev. B **81**, 235115 (2010).
[10] J. Wen, A. Rüegg, C.-C. J. Wang, and G. Fiete, Phys. Rev. B **82**, 075125 (2010).
[11] A. Rüegg and G. A. Fiete, Phys. Rev. B **83**, 165118 (2011).
[12] K. Ferhat and A. Ralko, Phys. Rev. B **89**, 155141 (2014).
[13] S.-L. Yu and J.-X. Li, Phys. Rev. B **85**, 144402 (2012).
[14] M. L. Kiesel and R. Thomale, Phys. Rev. B **86**, 121105(R) (2012).
[15] M. L. Kiesel, C. Platt, and R. Thomale, Phys. Rev. Lett. **110**, 126405 (2013).
[16] W.-S. Wang, Z.-Z. Li, Y.-Y. Xiang, and Q.-H. Wang, Phys. Rev. B **87**, 115135 (2013).
[17] B. R. Ortiz, L. C. Gomes, J. R. Morey, M. Winiarski, M. Bordelon, J. S. Mangum, I. W. H. Oswald, J. A. Rodriguez-Rivera, J. R. Neilson, S. D. Wilson, E. Ertekin, T. M. McQueen, and E. S. Toberer, Phys. Rev. Materials **3**, 094407 (2019).
[18] K. Jiang, T. Wu, J.-X. Yin, Z. Wang, M. Hasan, S. Wilson, X. Chen, and J. Hu, arXiv:2109.10809 [cond-mat.supr-con].
[19] Y.-X. Jiang, J.-X. Yin, M. Denner, N. Shumiya, B. Ortiz, G. Xu, Z. Guguchia, J. He, M. Hossain, X. Liu, J. Ruff, L. Kautzsch, S. S. Zhang, G. Chang, I. Belopolski, Q. Zhang, T. A. Cochran, D. Multer, M. Litskevich, Z.-J. Cheng *et al.*, Nat. Mater. **20**, 1353 (2021).
[20] H. Zhao, H. Li, B. Ortiz, S. Teicher, T. Park, M. Ye, Z. Wang, L. Balents, S. Wilson, and I. Zeljkovic, Nature (London) **599**, 216 (2021).
[21] E. Uykur, B. R. Ortiz, O. Iakutkina, M. Wenzel, S. Wilson, M. Dressel, and A. A. Tsirlin, Phys. Rev. B **104**, 045130 (2021).
[22] B. R. Ortiz, S. M. L. Teicher, L. Kautzsch, P. M. Sarte, N. Ratcliff, J. Harter, J. P. C. Ruff, R. Seshadri, and S. D. Wilson, Phys. Rev. X **11**, 041030 (2021).
[23] Z. Liang, X. Hou, F. Zhang, W. Ma, P. Wu, Z. Zhang, F. Yu, J.-J. Ying, K. Jiang, L. Shan, Z. Wang, and X.-H. Chen, Phys. Rev. X **11**, 031026 (2021).
[24] N. Shumiya, M. S. Hossain, J. X. Yin, Y. X. Jiang, B. R. Ortiz, H. Liu, Y. Shi, Q. Yin, H. Lei, S. S. Zhang, G. Chang, Q. Zhang, T. A. Cochran, D. Multer, M. Litskevich, Z. J. Cheng, X. P. Yang, Z. Guguchia, S. D. Wilson, and M. Z. Hasan, Phys. Rev. B **104**, 035131 (2021).
[25] H. Li, H. Zhao, B. Ortiz, T. Park, M. Ye, L. Balents, Z. Wang, S. Wilson, and I. Zeljkovic, Nat. Phys. **18**, 265 (2022).
[26] B. R. Ortiz, S. M. L. Teicher, Y. Hu, J. L. Zuo, P. M. Sarte, E. C. Schueller, A. M. Abeykoon, M. J. Krogstad, S. Rosenkranz, R. Osborn, R. Seshadri, L. Balents, J. He, and S. D. Wilson, Phys. Rev. Lett. **125**, 247002 (2020).
[27] B. R. Ortiz, P. M. Sarte, E. M. Kenney, M. J. Graf, S. M. L. Teicher, R. Seshadri, and S. D. Wilson, Phys. Rev. Materials **5**, 034801 (2021).
[28] Q. Yin, Z. Tu, C. Gong, Y. Fu, S. Yan, and H. Lei, Chin. Phys. Lett. **38**, 037403 (2021).
[29] H. Chen, H. Yang, B. Hu, Z. Zhao, J. Yuan, Y. Xing, G. Qian, Z. Huang, G. Li, Y. Ye, S. Ma, S. Ni, H. Zhang, Q. Yin, C. Gong, Z. Tu, H. Lei, H. Tan, S. Zhou, C. Shen *et al.*, Nature (London) **599**, 222 (2021).
[30] M. H. Christensen, T. Birol, B. M. Andersen, and R. M. Fernandes, Phys. Rev. B **104**, 214513 (2021).
[31] Y. Hu, X. Wu, B. Ortiz, X. Han, N. Plumb, S. Wilson, A. Schnyder, and M. Shi, arXiv:2201.06477 [cond-mat.supr-con].
[32] S. Yang, Y. Wang, B. Ortiz, D. Liu, J. Gayles, E. Derunova, R. Gonzalez-Hernandez, L. Smejkal, Y. Chen, S. Parkin, S. D. Wilson, E. S. Toberer, T. McQueen, and M. N. Ali, Sci. Adv. **6**, eabb6003 (2020).
[33] Z. Wang, Y.-X. Jiang, J.-X. Yin, Y. Li, G.-Y. Wang, H.-L. Huang, S. Shao, J. Liu, P. Zhu, N. Shumiya, M. S. Hossain, H. Liu, Y. Shi, J. Duan, X. Li, G. Chang, P. Dai, Z. Ye, G. Xu, Y. Wang *et al.*, Phys. Rev. B **104**, 075148 (2021).
[34] Q. Wu, Z. Wang, Q. Liu, R. Li, S. Xu, Q. Yin, C. Gong, Z. Tu, H. Lei, T. Dong, and N. L. Wang, arXiv:2110.11306 [cond-mat.supr-con].
[35] L. Yu, C. Wang, Y. Zhang, M. Sander, S. Ni, Z. Lu, S. Ma, Z. Wang, Z. Zhao, H. Chen, K. Jiang, Y. Zhang, H. Yang, F. Zhou, X. Dong, S. L. Johnson, M. J. Graf, J. Hu, H.-J. Gao, and Z. Zhao, arXiv:2107.10714 [cond-mat.supr-con].
[36] C. Mielke, D. Das, J.-X. Yin, H. Liu, R. Gupta, Y.-X. Jiang, M. Medarde, X. Wu, H. C. Lei, J. Chang, P. Dai, Q. Si, H. Miao, R. Thomale, T. Neupert, Y. Shi, R. Khasanov, M. Z. Hasan, H. Luetkens, and Z. Guguchia, Nature (London) **602**, 245 (2022).
[37] M. M. Denner, R. Thomale, and T. Neupert, Phys. Rev. Lett. **127**, 217601 (2021).
[38] M. Y. Jeong, H.-J. Yang, H. S. Kim, Y. B. Kim, S. Lee, and M. J. Han, Phys. Rev. B **105**, 235145 (2022).
[39] T. Park, M. Ye, and L. Balents, Phys. Rev. B **104**, 035142 (2021).
[40] Y.-P. Lin and R. M. Nandkishore, Phys. Rev. B **104**, 045122 (2021).
[41] X. Feng, K. Jiang, Z. Wang, and J. Hu, Sci. Bull. **66**, 1384 (2021).

[42] X. Feng, Y. Zhang, K. Jiang, and J. Hu, Phys. Rev. B **104**, 165136 (2021).
[43] T. Mertz, P. Wunderlich, S. Bhattacharyya, F. Ferrari, and R. Valentí, npj Comput. Mater. **8**, 66 (2022).
[44] H.-J. Yang, H. Kim, M. Jeong, Y. Kim, M. Han, and S. Lee, arXiv:2203.07365 [cond-mat.supr-con].
[45] M. Wenzel, B. R. Ortiz, S. D. Wilson, M. Dressel, A. A. Tsirlin, and E. Uykur, Phys. Rev. B **105**, 245123 (2022).
[46] Y. Xie, Y. Li, P. Bourges, A. Ivanov, Z. Ye, J.-X. Yin, M. Z. Hasan, A. Luo, Y. Yao, Z. Wang, G. Xu, and P. Dai, Phys. Rev. B **105**, L140501 (2022).
[47] N. Ratcliff, L. Hallett, B. R. Ortiz, S. D. Wilson, and J. W. Harter, Phys. Rev. Materials **5**, L111801 (2021).
[48] H. Tan, Y. Liu, Z. Wang, and B. Yan, Phys. Rev. Lett. **127**, 046401 (2021).
[49] H. Luo, Q. Gao, H. Liu, Y. Gu, D. Wu, C. Yi, J. Jia, S. Wu, X. Luo, Y. Xu, L. Zhao, Q. Wang, H. Mao, G. Liu, Z. Zhu, Y. Shi, K. Jiang, J. Hu, Z. Xu, and X. J. Zhou, Nat. Commun. **13**, 273 (2022).
[50] S. Wu, B. R. Ortiz, H. Tan, S. D. Wilson, B. Yan, T. Birol, and G. Blumberg, Phys. Rev. B **105**, 155106 (2022).
[51] G. Liu, X. Ma, K. He, Q. Li, H. Tan, Y. Liu, J. Xu, W. Tang, K. Watanabe, T. Taniguchi, L. Gao, Y. Dai, H.-H. Wen, B. Yan, and X. Xi, Nat. Commun. **13**, 3461 (2022).
[52] J.-W. Mei, F. Ye, and X. Chen, arXiv:2204.05216 [cond-mat.str-el].
[53] W. P. Su, J. R. Schrieffer, and A. J. Heeger, Phys. Rev. Lett. **42**, 1698 (1979).
[54] See Supplemental Material at http://link.aps.org/supplemental/10.1103/PhysRevB.106.L081107 for additional results concerning the purely electronic model.
[55] M. Capello, F. Becca, M. Fabrizio, S. Sorella, and E. Tosatti, Phys. Rev. Lett. **94**, 026406 (2005).
[56] M. Capello, F. Becca, S. Yunoki, and S. Sorella, Phys. Rev. B **73**, 245116 (2006).
[57] L. F. Tocchio, H. O. Lee, H. Jeschke, R. Valentí, and C. Gros, Phys. Rev. B **87**, 045111 (2013).
[58] L. F. Tocchio, C. Gros, X.-F. Zhang, and S. Eggert, Phys. Rev. Lett. **113**, 246405 (2014).
[59] R. Kaneko, L. F. Tocchio, R. Valentí, and C. Gros, Phys. Rev. B **94**, 195111 (2016).
[60] M. Bijelic, R. Kaneko, C. Gros, and R. Valentí, Phys. Rev. B **97**, 125142 (2018).
[61] S. Sorella, Phys. Rev. B **71**, 241103(R) (2005).
[62] O. Stauffert, M. Walter, M. Berciu, and R. V. Krems, Phys. Rev. B **100**, 235129 (2019).
[63] F. Ferrari, R. Valentí, and F. Becca, Phys. Rev. B **102**, 125149 (2020).
[64] F. Ferrari, R. Valentí, and F. Becca, Phys. Rev. B **104**, 035126 (2021).